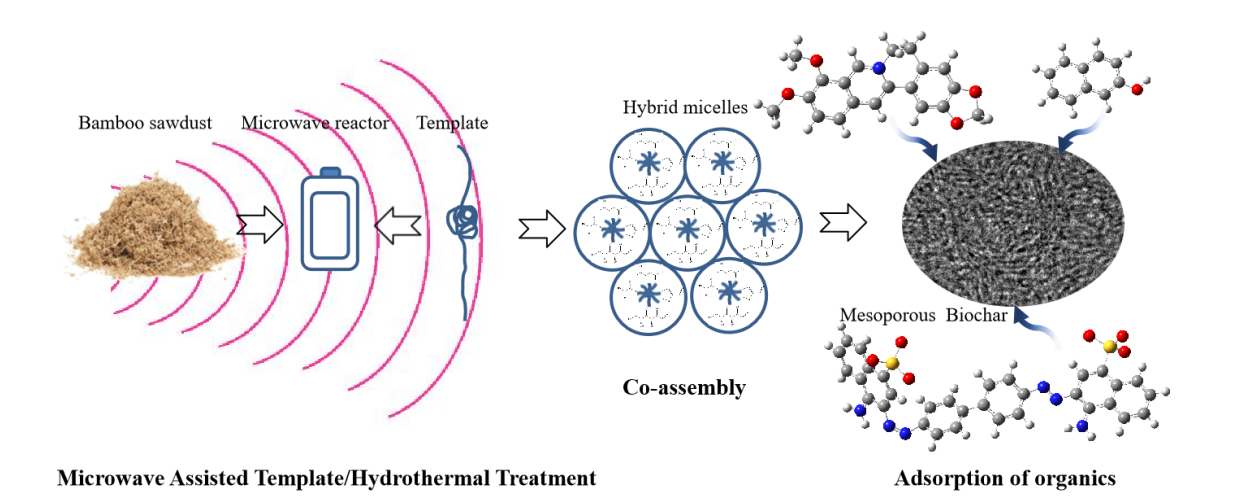
Mesoporous Bamboo Biochar from Microwave-assisted Template/Hydrothermal Treatment for Adsorption of Organics

Yin Li,^{a,*}, Xinyi Yu,^b Junfeng Zhang,^b Zengkun Wang,^b Tao Zhang,^b Jian Yang,^a Jun Dong,^a Shuqi Li,^a Chuang Xing,^b and Xikun Gai ^{b,*}

DOI: 10.15376/biores.20.3.6979-6999

GRAPHICAL ABSTRACT



^{*} Corresponding author: cherryli1986@126.com; gaixikun@163.com

Mesoporous Bamboo Biochar from Microwave-assisted Template/Hydrothermal Treatment for Adsorption of Organics

Yin Li,^{a,b*} Xinyi Yu,^b Junfeng Zhang,^b Zengkun Wang,^b Tao Zhang,^b Jian Yang,^a Jun Dong,^a Shuqi Li,^a Chuang Xing,^b and Xikun Gai ^{b,*}

Recycling of residual biomass in the form of carbonaceous materials is a sustainable and economically viable management option with zero net carbon dioxide emissions. Mesoporous bamboo biochars were produced via microwave-assisted hydrothermal/soft template treatment. Then they were characterized and evaluated for their adsorption capabilities for three organics. The biochars were found to have mesoporous structures with BET surface areas of 13.0 to 288 m²/g, total pore volumes in the range of 0.017 to 0.313 cm³/g, and average pore diameters between 4.0 and 6.7 nm in size. The surface areas and pore volumes were highly related to the hydrothermal treatment conditions. The mesoporous bamboo biochars showed adsorption amounts for 2-naphthol, berberine hydrocholoride, and Congo red in the range of 35.0 to 155.7, 76.1 to 129.6, 57.9 to 114.4 mg/g, respectively, at the adsorbate concentration of 0.5 mg/mL, and their adsorption capabilities depended on both the porosity and the surface groups. The adsorption of the three organics on the selected sample was a spontaneous and exothermic process with physical adsorption as the dominant mechanism. The adsorption could achieve equilibrium within 20, 40, and 60 min for 2-naphthol, berberine hydrochloride, and Congo red, respectively. This study provides a prospective method to produce biomass-derived mesoporous carbon adsorbents for adsorptive separation of organics from water.

DOI: 10.15376/biores.20.3.6979-6999

Keywords: Mesoporous biochar; Microwave; Hydrothermal carbonization; Adsorption

Contact information: a: Institute of Ecology & Health, Hangzhou Vocational & Technical College, Hangzhou 310018, Zhejiang, China; b: Zhejiang Provincial Key Lab for Chemical and Biological Processing Technology of Farm Product, School of Biological and Chemical Engineering, Zhejiang University of Science and Technology, Hangzhou 310023, Zhejiang, China;

INTRODUCTION

Biomass, such as agricultural and forestry wastes, as the only carbon-containing renewable resource, is a potential alternative to fossil fuels for producing fuels and chemicals with zero-carbon dioxide emissions (Wang *et al.* 2020), but it is still largely underutilized worldwide. Biomass-derived carbonaceous materials have found their wide applications in separation, energy, environment (Yin *et al.* 2023), and recycling agricultural and forestry wastes in the form of carbonaceous materials is a sustainable and economically viable management option (Campos *et al.* 2020). In addition, the increasing population and continuing economic and industrial development have contributed to levels of pollutants in drinking water, surface water, and groundwater, which harm the environment and human

^{*} Corresponding authors: cherryli1986@126.com; gaixikun@163.com

health (Lu and Astruc 2020; Vasseghian *et al.* 2021). Organic pollutants, including common industrial organic chemicals, dyes, pharmaceuticals, personal care products, pesticides, and so on are recalcitrant and persistent in the environment; some of them are highly toxic and can accumulate in food chain (Drout *et al.* 2019; Goh *et al.* 2025). The treatment of water polluted with organic matter is thus of special concern, and carbonaceous adsorbents have been widely used to remove various organic pollutants from aqueous solutions (Premarathna *et al.* 2019; Zhang *et al.* 2021).

Biochars are carbonaceous materials produced from direct pyrolysis and hydrothermal carbonization of biomass (Tekin et al. 2014; Zhao et al. 2018). The term "hydrochar" will be used in this article to denote related products prepared by hydrothermal treatment. Biochar of either type has been found to be effective in adsorbing organic pollutants from water (Liou et al. 2023; Liu et al. 2023). However, one of the limitations of biochar and hydrochar in organic adsorption is their poor textural properties, i.e. limited surface area per unit mass. Biochar from pyrolysis could have a surface area up to about 180 m²/g (Yang et al. 2019). While the properties of such carbonaceous materials depend on processing conditions, such as particle size of the feedstock, temperature, residence time, and heating procedure, the pore textural properties of biochar still highly depend on the original pore structure of the feedstock (Hyväluoma et al. 2018). Compared with pyrolysisderived biochar, hydrochar generally has relatively low porosity, which hinders its use in some applications (Kumar et al. 2020). Activation with physical and chemical methods is widely applied to increase the Brunauer-Emmett-Teller (BET) specific surface area of the biomass-derived chars (Boulanger et al. 2024); however, most of the activated carbons prepared via these methods do not have mesoporous structures with controlled pore sizes, and the pore structures dominated by micropores limit the application of the activated carbons in the adsorption of macromolecules, because steric effects play an important role in the adsorption of organics (Xiao and Pignatello 2015).

Tailoring the mesoporous structure of carbonaceous materials by a template method was first reported by Ryoo, Hyeon, and their coworkers in 1999 (Lee et al. 1999; Ryoo et al. 1999). In this method, carbonaceous materials with tunable mesoporous structures could be prepared using hard templates (e.g., mesoporous silicate materials) or soft templates (e.g., amphiphilic molecules) as structuring agents. Theoretically, in the soft template route, the carbon source should be able to form hydrogen bonds or Coulomb force interactions with the soft template to self-assemble into nanostructures, which then form a highly crosslinked polymer network to retain the mesoporous structures after the removal of poreforming component (Gang et al. 2021; Liang et al. 2008). Thus, only a few substances can be applied as carbon resources for the successful synthesis of mesoporous carbons through this approach. Biomass-derived compounds, such as D-fructose, cyclodextrin, tannin, and lignin (Jedrzejczyk et al. 2021) have been successfully used as carbon resources to produce mesoporous carbon through a soft template approach. Zheng and coworkers also reported the preparation of batatas-derived mesoporous biochar *via* soft-template method (Zheng *et* al. 2021). Batatas have been known to have high starch content, and the sugars from starch hydrolysis in hydrothermal environment have been widely reported to be used as carbon sources in mesoporous carbon production via the template method (Xiao et al. 2017). However, lignocellulosic biomass is a complex heterogeneous polymer; generally it cannot meet the mentioned requirements, and few literature is available regarding the possibility of producing mesoporous biochar by direct assembly between actual lignocellulosic biomass and soft templates.

In this study, microwave irradiation was employed to facilitate both the hydrothermal decomposition process and the co-assembly between degradation products and soft templates in one pot, enabling the direct production of mesoporous biochar from real lignocellulosic biomass and soft templates. Six bamboo-derived mesoporous biochar samples were produced. The effects of treatment temperature, time, and raw material composition on the physical and chemical properties of the chars were evaluated, and their adsorption properties for three organics from aqueous solutions were performed and analyzed in detail.

EXPERIMENTAL

Chemicals

Bamboo sawdust (with average dry mass content of 93.5 wt%) was obtained from a local market in Anji county, China. Pluronic F127 (PEO-PPO-PEO), 2- naphthol, berberine hydrochloride (BH), and Congo red (CR) were purchased from Shanghai Macklin Biochemical Co., Ltd.; and NaOH and ethanol were obtained from Shanghai Ling Feng Chemical Reagent Co., Ltd. All the reagents were analytical grade and used without further purification.

Preparation of Mesoporous Bamboo Biochar

As pretreatment, bamboo sawdust (2 g) was immersed in NaOH solution (2 mol/L, 20 mL) for 24 h at room temperature. The treated solid was then filtered off from the mixture, washed with distilled water repeatedly until a neutral pH supernatant, and then dried.

The pretreated bamboo sawdust was ground in a mortar together with a certain amount of F127 to produce a uniformly mixed powder. The mixture and 36 mL of 0.2 mol/L NaOH solution (or deionized water) were added together in a microwave reactor and heated at 100 or 140 °C for 50 or 80 min. The temperature 140 °C was selected as the main reaction condition by taking into comprehensive consideration the temperature required for the hydrothermal degradation of bamboo sawdust and the cloud point of F127. Additionally, a lower hydrothermal temperature is beneficial for obtaining a regular pore structure; therefore, 100 °C was chosen for comparison. Furthermore, a microwave reaction duration of 50 min was shown to be sufficient for the co-assembly reaction between the carbon source and templating agent, while a longer reaction time favors the degradation of biomass. Hence, 50 min and 80 min were selected as reaction times.

The detailed reaction conditions for each sample are listed in Table 1. The reactor was then cooled, and the obtained solid was dried. Finally, mesoporous bamboo biochar was acquired through calcination of the solid in nitrogen under 350 $^{\circ}$ C for 5 h and then at 900 $^{\circ}$ C for 4 h with a rate of 5 $^{\circ}$ C/min.

Samples	Temperature (°C)	Reaction Time (min)	Bamboo Sawdust: F127 (Mass Ratio)	Reaction Agent
1	140	50	1:1	0.2 mol/L NaOH
2	140	50	1:1	Deionized water
3	100	50	1:1	0.2 mol/L NaOH
4	140	50	1:2	0.2 mol/L NaOH
5	140	50	2:1	0.2 mol/L NaOH
6	140	80	2:1	0.2 mol/L NaOH

Table 1. Preparation Process Conditions of the Mesoporous Bamboo Biochars

Characterization

The Brunner-Emmet-Teller (BET) analysis of the mesoporous bamboo biochars was carried out on a Micromeritics ASAP 2020 system. The surface chemical compositions and functional groups of the samples were measured through X-ray photoelectron spectroscopy (XPS, Thermo Scientifc K-Alpha). A scanning electron microscope (SEM, ZEISS Sigma 300) was used to observe the surface morphology of the selected sample. A transmission electron microscope (TEM, Joel JEM-2100F) was employed to image the microstructure of the char sample.

Adsorption Thermodynamics

The prepared mesoporous bamboo biochar (0.01 g) was dispersed in organic solution (20 mL) with a certain initial concentration (0.1, 0.2, 0.3, 0.4, and 0.5 mg/mL), and agitated in a shaker at 298, 308, and 318 K for 6 h to adsorption-desorption balance. The organic concentration after adsorption, $C_{\rm e}$ (mg/mL), was determined by a UV-vis spectrophotometer for CR at 499 nm, BH at 345 nm, and 2-naphthol at 274 nm. The adsorption amount per unit mass of the adsorbent, $Q_{\rm e}$ (mg/g), was calculated according to Eq. 1,

$$Q_e = (C_0 - C_e) \cdot V / m \tag{1}$$

where V(mL) is the organic solution volume and m(g) is the mesoporous biochar mass.

The experimental plots were fitted by Langmuir and Freundlich models based on the Eqs. S1 and S2 provided in the Supplementary material.

Adsorption Kinetics

Ten triangle flasks containing 0.005 g of selected mesoporous biochar sample and 10 mL of organic solution (0.5 mg/mL) in each were shaken at 298 K. The solution was collected at 10, 20, 30, 40, 50, 60, 90, 120, 180, and 240 min. The organic concentration at time t, C_t (mg/mL), was analyzed, and the corresponding adsorption capacity, Q_t (mg/g), was calculated using Eq. 2:

$$Q_t = (C_0 - C_t) \cdot V / m \tag{2}$$

The obtained data were described using the pseudo-first- and second-order equations and intraparticle diffusion model (Weber-Morris equation) (Kasozi *et al.* 2010) shown in Eqs. S3 through S5 in the Supplementary material in the Appendix.

RESULTS AND DISCUSSION

Characterization of the Mesoporous Bamboo Biochar

Table 2 shows the specific surface area, pore volume, and average pore size of the mesoporous bamboo biochars. The biochar samples exhibited surface areas ranging from 13.0 to 288 m²/g, some of which were higher than that of mesoporous biochar derived from waste carton prepared through two-step carbonization method (249 m²/g) (Wang et al. 2024). The pore volumes were from 0.017 to 0.313 cm³/g. Both the surface area and the pore volume were significantly higher than those of bamboo hydrochars produced without templates (Li et al. 2016). Their average pore diameter was between 4.01 and 6.74 nm, which falls within the range of mesopore size. N₂ adsorption-desorption isotherms with obvious hysteresis loops and Barrett-Joyner-Halenda (BJH) pore size distributions displayed in Fig. S1 (in Supplementary material) and Fig. 1, respectively, further confirm the mesoporous structures and narrow pore size distributions of the biochar samples. The main pore structure of all the samples consisted of mesopores within the approximate range 3.4 to 3.9 nm. This was larger than that of mesoporous bamboo biochars prepared via an activation method (2.0 to 2.5 nm) (Ao et al. 2024). Such a pore size is expected to be more conducive to the diffusion and adsorption of large-sized molecules within the pore channels. The pore size distributions of the mesoporous biochar samples were significantly narrower than those of both mesoporous bamboo biochars prepared *via* activation and mesoporous biochar derived from waste carton through two-step carbonization (Wang et al. 2024; Ao et al. 2024), demonstrating the precision of the preparation method in pore size regulation. These results illustrate that microwave-assisted template/hydrothermal treatment could be a promising method to prepare lignocellulosic biomass-derived mesoporous biochars. Meanwhile, it can be seen from Table 2 that surface areas and pore volumes of the biochar samples were highly dependent on the process conditions. Compared with sample 2 prepared with deionized water as hydrothermal medium, sample 1 prepared in NaOH solution had higher surface area and larger pore volume. On the one hand, a weakly alkaline environment is suitable for the co-assembly between carbon precursor and soft template in hydrothermal preparation of mesoporous carbon (Liang et al. 2008). On the other hand, the delignification effect of NaOH (Rabemanolontsoa and Saka 2016) could result in the partial removal of lignin and thus enhance the accessibility of the template to the structural components of bamboo biomass, and these might increase the porosity of the final carbon product. Moreover, an alkaline environment could benefit the generation of intermolecular ester bonds between hemicelluloses and other components through saponification (Carvalheiro et al. 2008), and thus lead to a more highly cross-linked structure, which is necessary to ensure the stability of mesoporous biochar's pore structure after removing the template. Comparing the surface area of sample 1 with that of sample 3 (Table 2), it is apparent that higher hydrothermal treatment temperature could result in a higher surface area. It was shown in the authors' previous work that the rise in temperature (from 80 to 120 °C) had a slight negative effect on the specific surface area of mesoporous carbon with soluble phenolic resin as carbon source (Li et al. 2020) in a similar microwave aqueous synthesis process, and the different tendency in this study might be because of the decomposition of bamboo lignocellulose in hydrothermal environment. A series of reactions could occur in the hydrothermal treatment of lignocellulosic biomass. Watersoluble small molecules including sugars, furfural, and 5-hydroxymethylfurfural (HMF) released from the hydrolysis, dehydration, and decarboxylation of biomass (Fakkaew et al.

2015) can form hydrogen bonds with soft templates and have been used as carbon resources for mesoporous carbon production (Liang *et al.* 2008). A higher temperature may prompt a higher degree of the generation, dissolution, and consequent transformation of these intermediates (Khan *et al.* 2019) and benefit the formation of mesoporous structure of the final product. Among samples 1, 4, and 5, sample 5 having the lowest F127 content exhibited the highest BET surface area, while sample 4 with the highest F127 content had the lowest surface area (Table 2). Normally, a soft template is applied at a low concentration in mesoporous carbon preparation to obtain a highly ordered sample. Too high F127 composition might lead to an insufficient assembly and cause the macroscopic phase separation of the carbon resource and soft template after hydrothermal treatment, and these could be the reason for the low porosity of sample 4. It can be observed from the pore properties of sample 5 and 6 that longer reaction time had a slightly negative effect on both the BET surface area and pore volume of the mesoporous biochars. This result suggests that the co-assembly reaction related to pore development should reach equilibrium quickly in microwave-assisted/hydrothermal environment.

Bamboo **BET** Total Average Reaction Sawdust: Temp. Specific Pore Pore Samples Time F127 Reaction Agent Surface (°C) Volume Diameter (min) (Mass Area (m²/g) (cm³/g) (nm) Ratio) 140 50 0.2 mol/L NaOH 106.8 0.081 4.01 1 1:1 2 140 50 13.0 0.017 6.50 1:1 Deionized water 6.37 3 100 50 1:1 0.2 mol/L NaOH 40.3 0.089 140 50 1:2 87.2 0.116 6.74 4 0.2 mol/L NaOH 5 140 50 2:1 0.2 mol/L NaOH 287.7 0.313 6.42 6 140 80 2:1 0.2 mol/L NaOH 263.8 0.190 4.64

Table 2. Pore Properties of the Mesoporous Bamboo Biochars

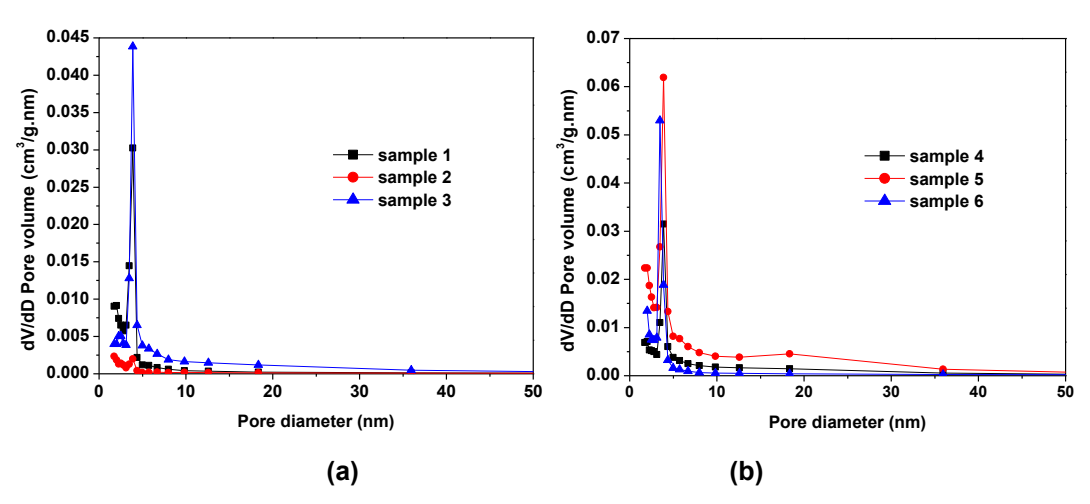
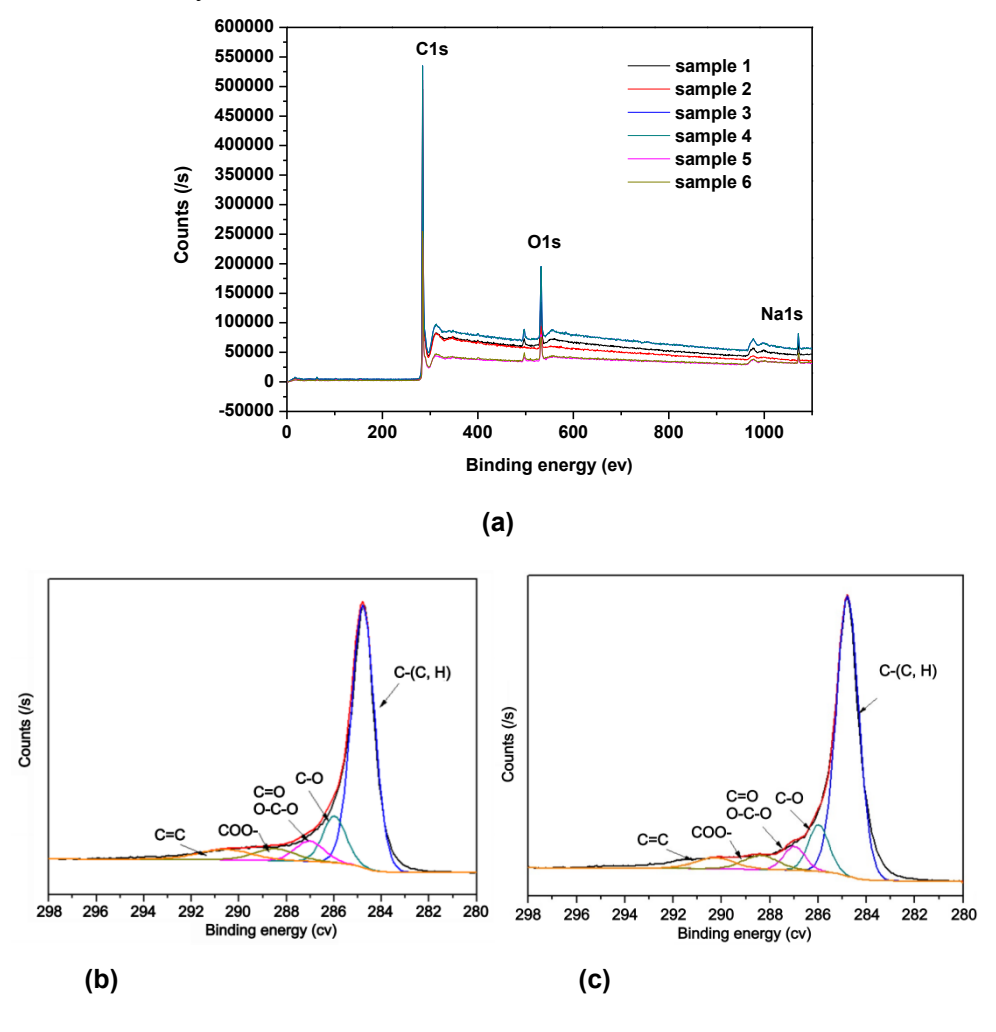


Fig. 1. Pore diameter distribution of the mesoporous bamboo biochars: (a) samples 1 through 3; (b) samples 4 through 6

The chemical composition and binding environment of the biochar samples from XPS spectra are displayed in Fig. 2. Figure 2a shows that the mesoporous bamboo biochars mainly contained C (284.8 eV) and O (531.8 eV), and samples 1 and 3 through 6 also

exhibited the characteristic peaks of Na (1072.0 eV), which should be a residue from the NaOH solution as reaction agent. As shown in Figs. 2b through 2g, C-(C, H) (284.5 eV), C-O (286 eV), C=O or O-C-O (286.8 eV), COO- (288.6 eV), and C=C (291.5 eV, $\pi \rightarrow \pi^*$ transitions in highly ordered and graphite structures) (Zhu et al. 2019) were the five carbon forms present on the surface of the mesoporous biochars, implying the presence of graphite-like carbon and O-containing functional including hydroxyl groups, ether groups, ester, and carboxyl groups on the samples. Relative area percentages of the carbon functionalities are listed in Table 3. The C-(C, H) areas of the samples were in the range of 61.5% to 73.0%, implying a hydrophobic surface of all these biochar samples. Different hydrothermal agents (deionized water and 0.2 mol/L NaOH) did not show remarkable influences on the carbon species, because samples 1 and 2 revealed guite similar carbon environments. Sample 3 prepared at a lower temperature of 100 °C showed a slightly lower graphitic character with lower intensity of C-(C, H) and higher relative area of C-O compared to sample 1 prepared at 140 °C, indicating that hydrothermal temperature could slightly influence the carbonization degree of the final char products. A marked decline in C-(C, H) area along with an increment in C-O area could be observed in sample 4 prepared with the highest soft template ratio compared to sample 1 and 5, which should be attributed to the higher oxygen content of F127 than that of bamboo sawdust. Sample 6 displays higher C-(C, H) content and lower C-O concentration than sample 5, which could be due to the more severe decomposition of bamboo sawdust's lignocellulose at a longer microwave assisted hydrothermal treatment time.



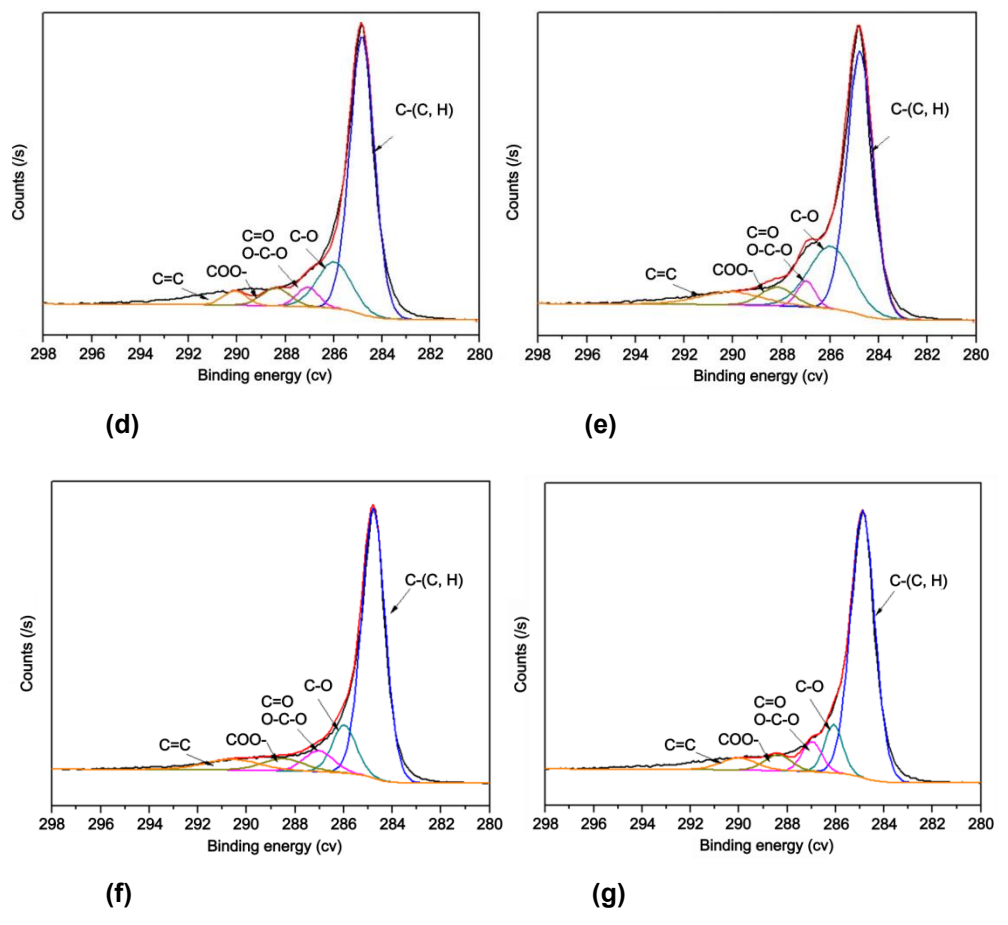
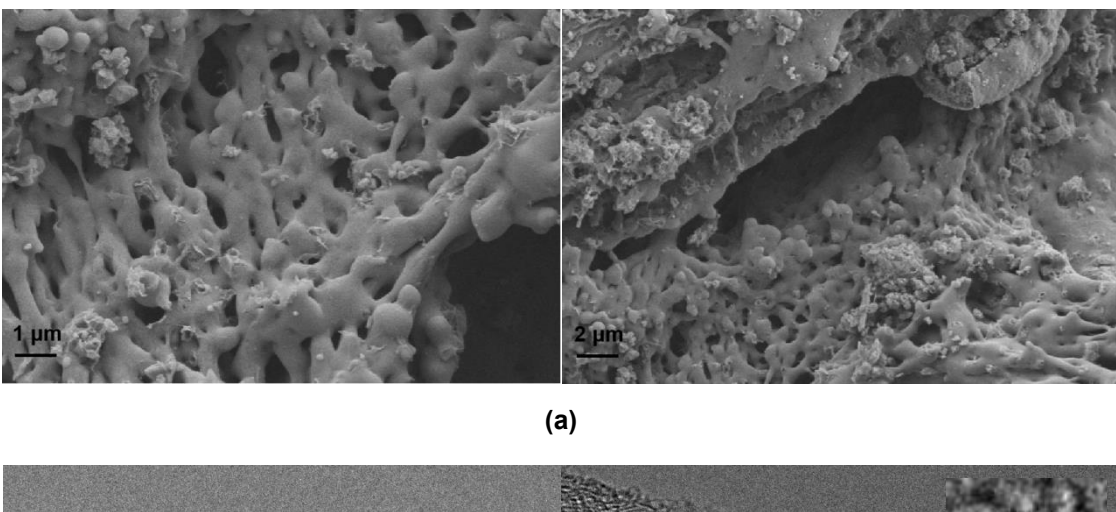


Fig. 2. (a) XPS survey; (b-g) C1s fits of the bamboo derived mesoporous carbon sample 1-6

Table 3. Relative Atomic Concentration of C in the Mesoporous Bamboo Biochars

Sample	C-(C, H) (%)	C-O (%)	C=O O-C-O (%)	COO- (%)	C=C (%)
Sample 1	73.0	11.0	6.8	6.3	2.9
Sample 2	72.0	11.0	6.0	5.9	5.2
Sample 3	70.8	16.1	4.4	5.3	3.4
Sample 4	61.5	22.7	3.9	5.2	6.8
Sample 5	68.4	12.4	6.9	5.8	6.6
Sample 6	73.0	10.0	6.8	5.1	5.1

Unlike the smooth and non-porous surface of the bamboo sawdust feedstock reported in the previous work (Li *et al.* 2023), mesoporous bamboo biochar sample 5 displayed obvious macroscopic pores, as shown in Fig. 3(a), compared to bamboo hydrochars produced without templates (Li *et al.* 2016). Homogeneous, wormlike but disordered porous structures could be observed throughout the whole biochar sample from its TEM images (Fig. 3(b)), while some highly ordered pore structures could also be seen locally (Fig. 3(b)). These results further confirm that microwave assisted template/hydrothermal treatment could be a prospective method to prepare mesoporous carbon from lignocellulosic biomass.



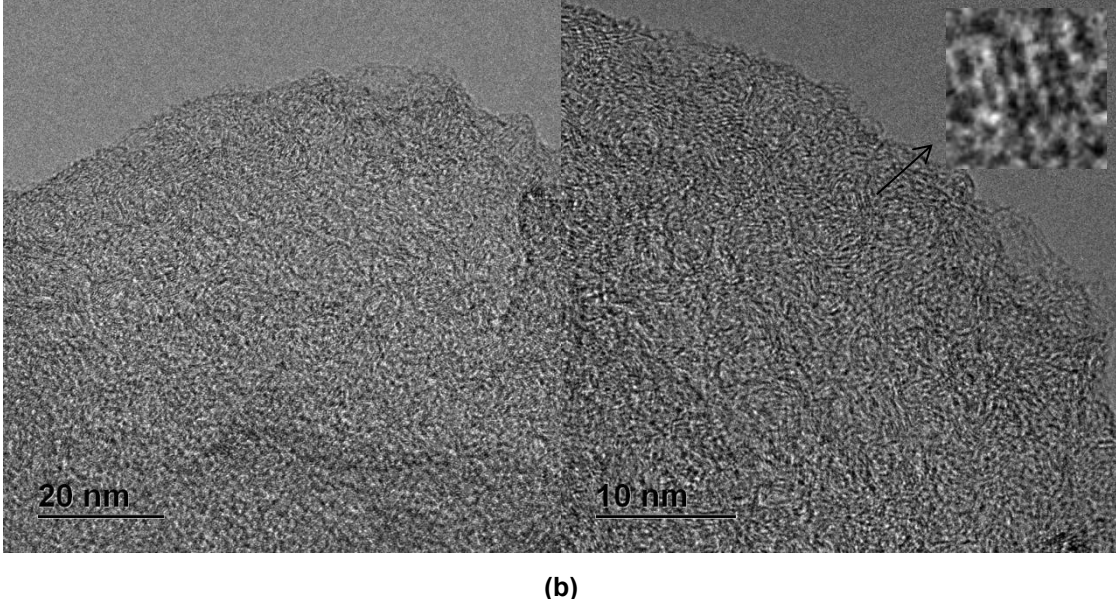


Fig. 3. SEM (a) and TEM (b) images of sample 5

Adsorption Isotherms and Thermodynamics

The experimental adsorption isotherm plots of 2-naphthol, BH, and CR on the carbon samples and the corresponding isotherm curves predicted from Langmuir and Freundlich equations are presented in Figs. 4a through 4c. It is observed that the mesoporous bamboo biochars had different adsorption abilities for the three adsorbates. The adsorption capacities at the initial concentration of 0.5 mg/mL for 2-naphthol, BH, and CR on the biochar samples were in the range of 35.0 to 155.7, 76.1 to 129.6, and 57.9 to 114.4 mg/g, respectively, and the adsorption amounts of 2-naphthol and CR on most of the mesoporous biochars were higher than those on bamboo hydrochars (Li et al. 2016). Compared to bamboo hydrochars, most of the mesoporous biochars prepared in this study exhibited richer mesoporous pores and higher surface areas that should benefit the adsorption for organics. Meanwhile, their more hydrophobic surface should enable different adsorption mechanisms. In contrast, the adsorption amounts of CR on the mesoporous biochars were much higher than those on activated carbon prepared from coir pith reported in literature (Namasivayam and Kavitha 2002), and it was reported that CR could block micropores (Pelekani and Snoeyink 2001); it could be inferred that mesoporous structure is favorable for the adsorption of organics larger in size such as CR.

Among all the biochar samples, sample 5 presented the highest adsorption capabilities for all the three organics, which might be attributed to its highest surface area and pore volume. However, sample 6 with the second largest surface area did not show comparable adsorption capacities. In contrast, sample 4 with a quite low specific surface area displayed relatively high adsorption amounts for the organics among all the carbon samples except sample 5, which could be due to its more abundant oxygen-containing functional groups than the other samples (Table 2). Both Sample 1 and Sample 6 exhibited quite low adsorption capacities for BH and CR (Fig. 4b and 4c). The molecular dimensions of 2naphthol, BH, and CR were calculated to be approximately 0.80 nm \times 0.53 nm, 1.47 nm \times $0.66 \text{ nm} \times 0.32 \text{ nm}$, and $2.29 \text{ nm} \times 0.82 \text{ nm} \times 0.60 \text{ nm}$, respectively (Li et al. 2013). This result may be attributed to the samples' smaller pore size, which can easily be blocked by the larger organic molecules. These results suggest that the adsorption capacities of the organics on the mesoporous bamboo biochars depend on both the pore properties and functional groups of the biochar samples. Specifically, a high surface area indicates an abundance of adsorption sites, while surface functional groups can facilitate weak intermolecular interactions, such as hydrogen bonding, between the adsorbent surface and organics. Furthermore, pore diameter plays a crucial role in the adsorption of organics with larger molecular sizes. The adsorption isotherm curves of 2-naphthol on samples 1 through 4 are near-linear (Fig. 4a), indicating a partition-involved adsorption mechanism (Chiou et al. 2015) and a low adsorption affinity.

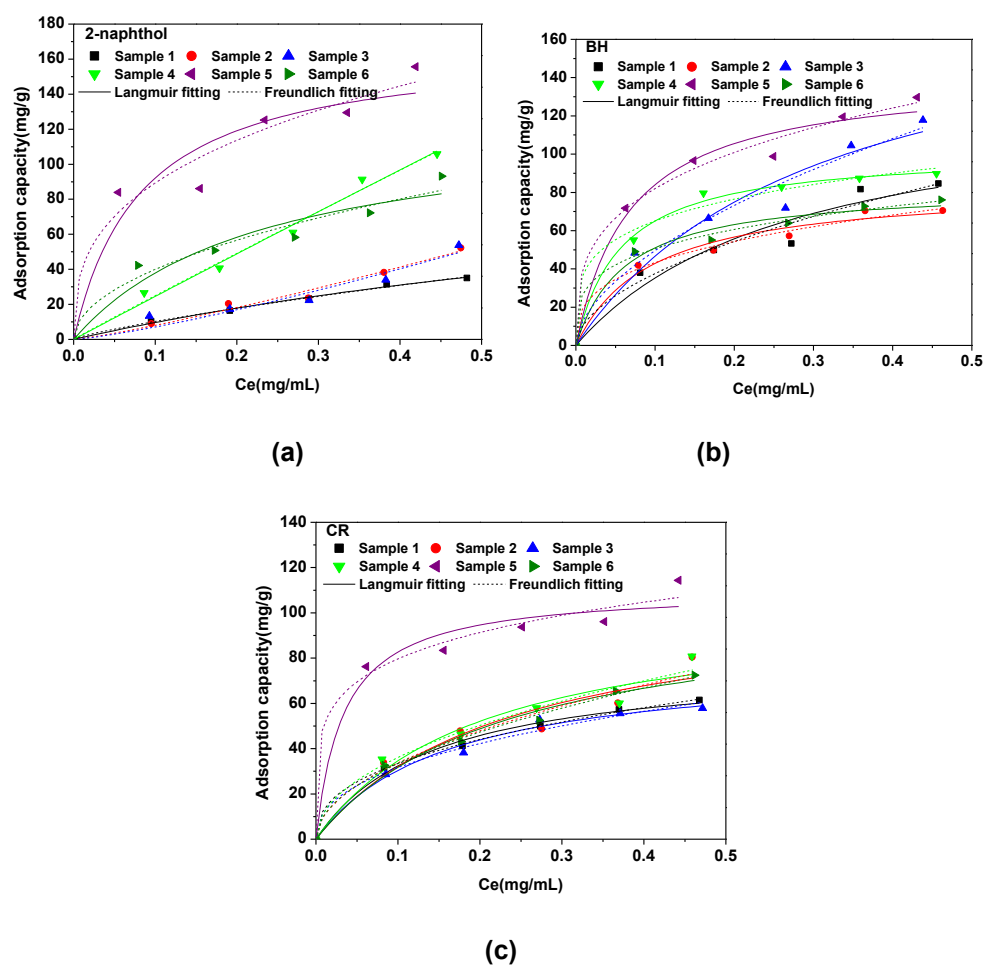
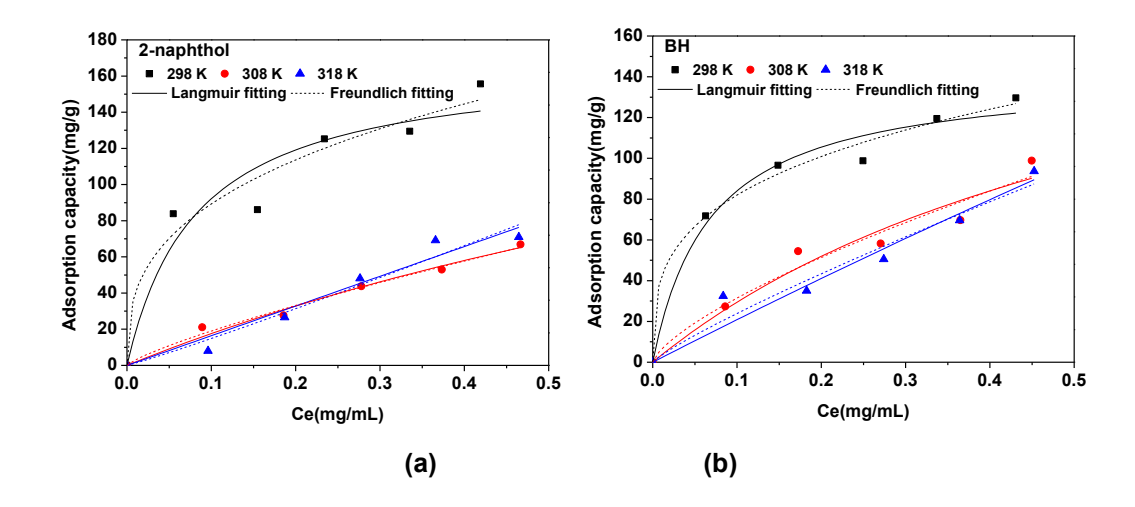


Fig. 4. Experimental adsorption isotherm plots and fit curves of 2-naphthol, BH, and CR on the mesoporous bamboo biochars at 298 K

The Freundlich model fit the experimental data better (with R^2 values between 0.941 and 0.995) than the Langmuir model for all the three organics on most of the mesoporous bamboo biochar samples, implying a heterogenous surface of the adsorbent and a physical adsorption dominated adsorption process. The Langmuir equation failed to describe the adsorption of 2-naphthol on mesoporous biochar sample 2 and 3, which should be attributed to the near linear shape of these adsorption isotherms. The 1/n value from the Freundlich model for these two adsorption isotherms was higher than 1, implying unfavorable adsorption processes in these cases.

Mesoporous bamboo biochar sample 5 presenting the highest surface area and the largest adsorption amounts for all the tested organics was selected for the further tests. Figure 5 gives the experimental adsorption isotherm data points as well as fit curves of 2naphthol, BH, and CR on sample 5 at 298, 308, and 318 K. The adsorption capacities of all the three organics decreased with the increment of temperature, while the $K_{\rm L}$ values from the Langmuir model decreased and 1/n values from the Freundlich model increased, indicating a decreasing adsorption affinity with the increasing temperature. This further confirms the physisorption dominated adsorption mechanism for the organics on the selected mesoporous bamboo biochar. The mesoporous biochars prepared in this study provided hydrophobic surfaces, but they still had small amounts of O-containing functional groups on their surfaces (Table 2). These could contribute to physisorption for organics through hydrophobic interactions and hydrogen bonds, and the presence of mesopores also determines the possibility of the pore-filling mechanism in the adsorption (Abbas et al. 2018). Meanwhile, the surface chemistry (Fig.2) of the biochar samples did not reveal chemisorption sites to form covalent bonds with organics. These reveal the physisorption dominated adsorption mechanism. In contrast, the oxygen-containing functional groups also indicated that the mesoporous biochar contained a certain proportion of noncarbonized fractions, which could contribute to the partition mechanism for the adsorption of organics. During partitioning, organics could solubilize within the matrix of organic matter of the mesoporous biochar to enhance the adsorption (Abbas et al. 2018). At higher adsorption temperatures of 308 and 318 K, physical interactions weaken, and the partition mechanism becomes dominant, which should be the reason for the nearly linear shapes of the adsorption isotherms.



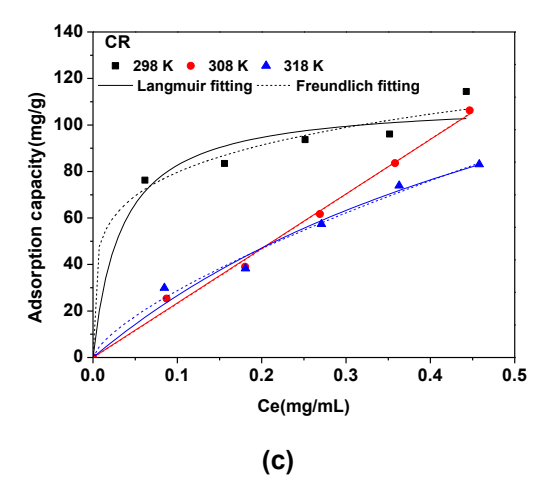


Fig. 5. Experimental adsorption isotherm plots and fit curves of 2-naphthol, BH, and CR on sample 5 at three temperatures

The changes in adsorption enthalpy (ΔH) , free energy (ΔG) , and entropy (ΔS) were calculated through the Van't Hoff equation for each organic on sample 5, to further illustrate the nature of the adsorption process, and the values were collected in Table 4. The negative free energy changes with absolute values less than 40 kJ/mol and negative enthalpy values suggest a spontaneous and exothermic adsorption process with physical adsorption as the predominant mechanism for all the three organics (Nuengmatcha et al. 2014). Such interactions should be mainly driven by van der Waals forces, π - π interactions, and electrostatic interactions. Physical adsorption is significantly influenced by specific surface area and pore size, surface area determines the number of adsorption sites, directly affecting adsorption capacity, while pore size determines whether adsorbate molecules can access the internal pores and further influences adsorption kinetics and selectivity. Optimal adsorption performance requires a combination of high specific surface area and appropriate pore size distribution. This agrees with the inferences derived from the adsorption capacity data. The negative ΔS values denoting the decrease in randomness should be attributed to the transition from three-dimensional motion to two-dimensional movement of the adsorbates after adsorption.

 Table 4. Thermodynamic Parameters for Each Adsorbates on Sample 5

Adsorbate		ΔG (kJ/mol)		ΔΗ	ΔS
Ausorbate	298 K	308 K	318 K	(kJ/mol)	(KJ/mol.K)
2-naphthol	-4.895	-4.318	-3.982	-18.47	-0.046
BH	-4.851	-4.534	-4.641	-7.912	-0.011
CR	-4.857	-4.401	-4.658	-7.715	-0.010

Adsorption Kinetics

The measurements of adsorption kinetic plots and corresponding fit curves of 2-naphthol, BH, and CR on mesoporous biochar sample 5 at 298 K are shown in Fig. 6. The organics were adsorbed rapidly on the mesoporous biochar, and the adsorption could reach equilibrium within 20 min for 2-naphthol, 40 min for BH, and 60 min for CR. The time was proportional to the molecular size of the adsorbates, which reveals the effect of pore diffusion on the adsorption rate.

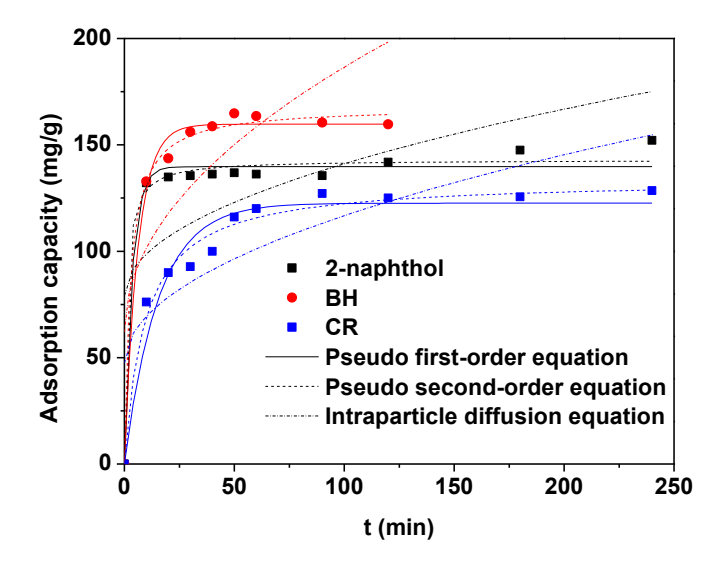


Fig. 6. Adsorption kinetics of 2-naphthol, BH, and CR on sample 5 at 298 K

The results indicate that the pseudo-second-order model best fit the experimental kinetic data ($R^2 > 0.981$) for all the three organics, while the intraparticle diffusion model showed the lowest R^2 values <0.690). It was reported that sorption behavior that fits the pseudo-second-order equation well can usually be attributed to diffusion-based mechanisms (Hubbe *et al.* 2019; Hubbe 2021). The sizes of the three organics were all smaller than the average pore size of sample 5, which was 6.6 nm (Table 2). It could also be observed that the R^2 values of the intraparticle diffusion model followed the order: $R^2_{2-\text{naphthol}} < R^2_{BH} < R^2_{CR}$, which is consistent with the molecular size order of the three adsorbates. These indicate that diffusion is the true rate-limiting step in this study, and with the increasing molecular size of the adsorbates, steric hindrance might become more important in adsorption kinetics.

CONCLUSIONS

- 1. The results support the usage of microwave assisted template/hydrothermal treatment as an efficient approach to produce mesoporous biochars from directly assembly between lignocellulosic biomass and soft template. Such chars may serve as potential sorbents for removing or separating organics from water.
- 2. The prepared mesoporous biochars exhibited notable pore properties (BET surface area: 13.0 to 287.7 m²/g, pore volume: 0.017 to 0.313 cm³/g, average pore diameter: 4.01 to 6.74 nm) and small amounts of O-containing functional groups. Process conditions, including synthesis composition, temperature, reaction time, and reaction agent, clearly affected the physical and chemical properties of the biochars and their adsorption capabilities for organics.
- 3. The mesoporous bamboo biochars accommodated adsorption quantities for 2-naphthol, berberine hydrocholoride, and Congo red in the range of 35.0 to 155.7, 76.1 to 129.6, and 57.9 to 114.4 mg/g, respectively, at the initial concentration of 0.5 mg/mL.

4. Sample 5, prepared at 140°C for 50 minutes with a mass ratio of bamboo sawdust to F127 at 2:1, exhibits the highest surface area and the greatest adsorption capacity for all three organic compounds. On this sample, the adsorption is spontaneous and exothermic with physical adsorption as the predominant mechanism for all the tested organics, and is also fast.

ACKNOWLEDGMENTS

The authors are grateful for the support of the National Natural Science Foundation of China, Grant No. 22208306, the Leading Talents Program of Zhejiang Province, Grant No. 2023C04021, and the State Key Laboratory of Heavy Oil Processing, Grant No. SKLHOP202202002.

REFERENCES CITED

- Abbas, Z., Ali, S., Rizwan, M., Zaheer, I.E., Malik, A., Riaz, M. A., Shahid, M. R., Rehman, M. Z., and Al-Wabel, M. I. (2018). "A critical review of mechanisms involved in the adsorption of organic and inorganic contaminants through biochar," *Arab. J. Geosci.* 11, article 448. DOI: 10.1007/s12517-018-3790-1
- Ao, W., Mian, M. M., and Zhang, Q. (2024). "Bamboo-derived low-cost mesoporous biochar for efficient removal of per- and polyfluoroalkyl substances from contaminated water," *ACS EST Water* 4(6), 2711-2720. DOI: 10.1021/acsestwater.4c00211
- Baseri, R., Palanisamy, P. N., and Kumar, P. (2012). "Adsorption of basic dyes from synthetic textile effluent by activated carbon prepared from *Thevetia peruviana*," *Indian J. Chem. Techn.* 19, 311-321.
- Boulanger, N., Talyzin, A. V., Xiong, S., Hultberg, M., and Grimm, A. (2024). "High surface area activated carbon prepared from wood-based spent mushroom substrate for supercapacitors and water treatment," *Colloid. Surface. A* 680, article ID 132684. DOI: 10.1016/j.colsurfa.2023.132684
- Campos, P., Miller, A. Z., Knicker, H., Costa-Pereira, M. F., Merino, A., and De la Rosa, J. M. (2020). "Chemical, physical and morphological properties of biochars produced from agricultural residues: Implications for their use as soil amendment," *Waste Manag.* 105, 256-267. DOI: 10.1016/j.wasman.2020.02.013
- Carvalheiro, F., Duarte, L. C., and Gírio, F.M. (2008). "Hemicellulose biorefineries: A review on biomass pretreatments," *J. Sci. Ind. Res.* 67(11), article ID 115030. DOI: 10.1088/0960-1317/18/11/115030
- Chiou, C. T., Cheng, J., Hung, W. N., Chen, B., and Lin, T. F. (2015). "Resolution of adsorption and partition components of organic compounds on black carbons," *Environ. Sci. Technol.* 49, 9116-9123. DOI: 10.1021/acs.est.5b01292
- Drout, R. J., Robison, L., Chen, Z., Islamoglu, T., and Farha, O. K. (2019). "Zirconium metal-organic frameworks for organic pollutant adsorption," *Trends Chem.* 1, 304-317. DOI: 10.1016/j.trechm.2019.03.010
- Fakkaew, K., Koottatep, T., and Polprasert, C. (2015). "Effects of hydrolysis and carbonization reactions on hydrochar production," *Bioresource Technol.* 192, 328-334. DOI: 10.1016/10.1016/j.biortech.2015.05.091

- Gang, D., Ahmad, Z. U., Lian, Q., Yao, L., and Zappi, M. E. (2021). "A review of adsorptive remediation of environmental pollutants from aqueous phase by ordered mesoporous carbon," *Chem. Eng. J.* 403, article ID 126286. DOI: 10.1016/j.cej.2020.126286
- Goh, S. W., Ng, Q. H., Rahim, S. K. E. A., Low, S. C., Hoo, P. Y., Yeo, R. Y. Z., Chew, T. L., and Jawad, Z. A. (2025). "Recent advancements in smart materials for the removal of organic, inorganic and microbial pollutants in water treatment: A review," *J. Water Process. Eng.* 70, article 106993. DOI: 10.1016/j.jwpe.2025.106993
- Hubbe, M. A. (2021). "Insisting upon meaningful results from adsorption experiments," *Sep. Purif. Rev.* 51(2), 212-225, article ID LSPR 1888299. DOI: 10.1080/15422119.2021.1888299
- Hubbe, M. A., Azizian, S., and Douven, S. (2019). "Implications of apparent pseudo-second-order adsorption kinetics onto cellulosic materials: A review," *BioResources* 14(3), 7582-7626. DOI: 10.15376/biores.14.3.7582-7626
- Hyväluoma, J., Hannula, M., Arstila, K., Wang, H., Kulju, S., and Rasa, K. (2018). "Effects of pyrolysis temperature on the hydrologically relevant porosity of willow biochar," *J. Anal. Appl. Pyrol.* 134, 446-453. DOI: 10.1016/j.jaap.2018.07.011
- Kasozi, G. N., Zimmerman, A. R., Nkedi-Kizza, P., and Gao, B. (2010). "Catechol and humic acid sorption onto a range of laboratory-produced black carbons (biochars)," *Environ. Sci. Technol.* 44, 6189-6195. DOI: 10.1021/es1014423
- Khan, T. A., Saud, A. S., Jamari, S. S., Rahim, M. H. A., Park, J. W., and Kim, H. J. (2019). "Hydrothermal carbonization of lignocellulosic biomass for carbon rich material preparation: A review," *Biomass Bioenerg*. 130, article ID 105384. DOI: 10.1016/j.biombioe.2019.105384
- Kumar, A., Saini, K., and Bhaskar, T. (2020). "Hydochar and biochar: Production, physicochemical properties and techno-economic analysis," *Bioresour. Technol.* 310, article 123442. DOI: 10.1016/j.biortech.2020.123442
- Lee, J., Yoon, S., Hyeon, T., Oh, S. M., and Kim, K. B. (1999). "Synthesis of a new mesoporous carbon and its application to electrochemical double-layer capacitors," *Chem. Commun.* 1999(21), 2177-2178. DOI: 10.1039/A906872D
- Li, Y., Cao, R., Wu, X., Huang, J., Deng, S., and Lu, X. (2013). "Hypercrosslinked poly(styrene-co-divinylbenzene) resin as a specific polymeric adsorbent for purification of berberine hydrochloride from aqueous solutions," *J. Colloid Interf. Sci.* 400, 78-87. DOI: 10.1016/j.jcis.2013.03.011
- Li, Y., Cheng, M., Jiang, Y. G., Pan, G. X., Wang, H. P., and Shan, S. D. (2020). "Microwave aqueous synthesis of mesoporous carbons for highly effective adsorption of berberine hydrochloride and matrine," *J. Inorg. Organomet. P.* 30, 2551-2561. DOI: 10.1007/s10904-019-01411-w
- Li, Y., Meas, A., Shan, S., Yang, R., and Gai, X. (2016). "Production and optimization of bamboo hydrochars for adsorption of Congo red and 2-naphthol," *Bioresource Technol.* 207, 379-386. DOI: 10.1016/j.biortech.2016.02.012
- Li, Y., Xu, Z., Zhang, Q., Di, J., Yang, R., Gai, X., Wang, H., and Zhang, T. (2023). "Mesoporous biochar derived from bamboo waste: Template/hydrothermal preparation and highly efficient pharmaceutical adsorption," *BioResources* 18(1), 1882-1900. DOI: 10.15376/biores.18.1.1882-1900
- Liang, C., Li, Z., and Dai, S. (2008). "Mesoporous carbon materials: Synthesis and modification," *Angew. Chem. Int. Edit.* 47, 3696-3717. DOI: 10.1002/anie.200702046

- Liou, T. H., Tseng, Y. K., Zhang, T. Y., Liu, Z. S., and Chen, J. Y. (2023). "Rice husk char as a sustainable material for the preparation of graphene oxide-supported biocarbons with mesoporous structure: A characterization and adsorption study," *Fuel* 344, Article ID 128042. DOI: 10.1016/j.fuel.2023.128042
- Liu, S., Wu, S., and Cheng, H. (2023). "Preparation and characterization of lignin-derived nitrogen-doped hierarchical porous carbon for excellent toluene adsorption performance," *Ind. Crop. Prod.* 192, Article ID 116120. DOI: 10.1016/j.indcrop.2022.116120
- Lu, F., and Astruc, D. (2020). "Nanocatalysts and other nanomaterials for water remediation from organic pollutants," *Coordin. Chem. Rev.* 408, Article ID 213180. DOI: 10.1016/j.ccr.2020.213180
- Namasivayam, C., and Kavitha, D. (2002). "Removal of Congo Red from water by adsorption onto activated carbon prepared from coir pith, an agricultural solid waste," *Dyes. Pigments* 54, 47-58. DOI: 10.1016/S0143-7208(02)00025-6
- Nuengmatcha, P., Mahachai. R., and Chanthai. S. (2014). "Thermodynamic and kinetic study of the intrinsic adsorption capacity of graphene oxide for malachite green removal from aqueous solution," *Orient. J. Chem.* 30, 1463-1474. DOI: 10.13005/ojc/300403
- Pelekani, C., and Snoeyink, V. L. (2001). "A kinetic and equilibrium study of competitive adsorption between atrazine and Congo red dye on activated carbon: The importance of pore size distribution," *Carbon* 39, 25-37. DOI: 10.1016/S0008-6223(00)00078-6
- Premarathna, K. S. D., Upamali Rajapaksha, A., Sarkar, B., Kwon, E. E., Bhatnagar, A., Sik Ok, Y., and Vithanage, M. (2019). "Biochar-based engineered composites for sorptive decontamination of water: A review," *Chem. Eng. J.* 372, 536-550. DOI: 10.1016/j.cej.2019.04.097
- Rabemanolontsoa, H., and Saka, S. (2016). "Various pretreatments of lignocellulosics," *Bioresource Technol.* 199, 83-91. DOI: 10.1016/j.biortech.2015.08.029
- Ryoo, R., Joo, S. H., and Jun, S. (1999). "Synthesis of highly ordered carbon molecular sieves *via* template-mediated structural transformation," *J. Phys. Chem. B* 103, 7743-7746. DOI: 10.1021/jp991673a
- Tekin, K., Karagöz, S., and Bektaş, S. (2014). "A review of hydrothermal biomass processing," *Renew. Sust. Energ. Rev.* 40, 673-687. DOI:10.1016/j.rser.2014.07.216
- Vasseghian, Y., Sevda Hosseinzadeh, S., Alireza Khataee, A., and Elena-Niculina Dragoi, E. N. (2021). "The concentration of persistent organic pollutants in water resources: A global systematic review, meta-analysis and probabilistic risk assessment," *Sci. Total Environ.* 796, Article ID 149000. DOI: 10.1016/j.scitotenv.2021.149000
- Wang, Y., Hu, Y. J., Hao, X., Peng, P., and Sun, R. C. (2020). "Hydrothermal synthesis and applications of advanced carbonaceous materials from biomass: A review," *Adv. Compos. Hybrid Ma.* 3, 267-284. DOI: 10.1007/s42114-020-00158-0
- Wang, Y., Huo, T., Wang, Y., Bai, J., Huang, P., Li, C., Deng, S., Mei, H., Qian, J., Zhang, Q., and Wang, W. (2024). "Constructing mesoporous biochar derived from waste carton: improving multi-site adsorption of dye wastewater and investigating mechanism," *Environ. Res.* 242(2024), article 117775. DOI: 10.1016/j.envres.2023.117775

- Xiao, F., and Pignatello, J. J. (2015). "Interactions of triazine herbicides with biochar: Steric and electronic effects," *Water Res.* 80, 179-188. DOI: 10.1016/j.watres.2015.04.040
- Xiao, P. W., Zhao, L., Sui, Z. Y., Xu, M. Y., and Han, B. H. (2017). "Direct synthesis of ordered mesoporous hydrothermal carbon materials *via* a modified soft-templating method," *Micropor. Mesopor. Mat.* 253, 215-222. DOI: 10.1016/j.micromeso.2017.07.001
- Yin. Y., Liu. Q., Zhao. Y., Chen. T., Wang, J., Gui, L., and Lu. C. (2023). "Recent progress and future directions of biomass-derived hierarchical porous carbon: Designing, preparation, and supercapacitor applications," *Energy Fuels* 37(5), 3523-3554. DOI: 10.1021/acs.energyfuels.2c04093
- Zhang, J., Zhang, N., Tack, F. M. G., Sato, S., Alessi, D. S., Oleszczuk, P., Wang, H., Wang, X., and Wang, S. (2021). "Modification of ordered mesoporous carbon for removal of environmental contaminants from aqueous phase: A review," *J. Hazard. Mater.* 418, Article ID 126266. DOI: 10.1016/j.jhazmat.2021.126266
- Zhao, B., O'Connor, D., Zhang, J., Peng, T., Shen, Z., Tsang, D.C.W., and Hou, D. (2018). "Effect of pyrolysis temperature, heating rate, and residence time on rapeseed stem derived biochar," *J. Clean. Prod.* 174, 977-987. DOI: 0.1016/j.jclepro.2017.11.013
- Zheng, Z., Zhao, B., Guo, Y., Guo, Y., Pak, T., and Li, G. (2021b). "Preparation of mesoporous batatas biochar *via* soft-template method for high efficiency removal of tetracycline," *Sci. Total Environ.* 787, Article ID 147397. DOI: 10.1016/j.scitotenv.2021.147397
- Zhu, G., Yang, L., Gao, Y., Xu, J., Chen, H., Zhu, Y., Wang, Y., Liao, C., Lu, C., and Zhu, C. (2019). "Characterization and pelletization of cotton stalk hydrochar from HTC and combustion kinetics of hydrochar pellets by TGA," *Fuel* 244, 479-491. DOI: 10.1016/j.fuel.2019.02.039

Article submitted: November 21, 2024; Peer review completed: January 11, 2025; Revisions accepted: May 20, 2025; Published: June 27, 2025.

DOI: 10.15376/biores.20.3.6979-6999

APPENDIX

Langmuir equation:
$$Q_e = \frac{Q_m K_L C_e}{1 + K_L C_e}$$
 (S1)

Freundlich equation:
$$Q_e = K_F C_e^{1/n}$$
 (S2)

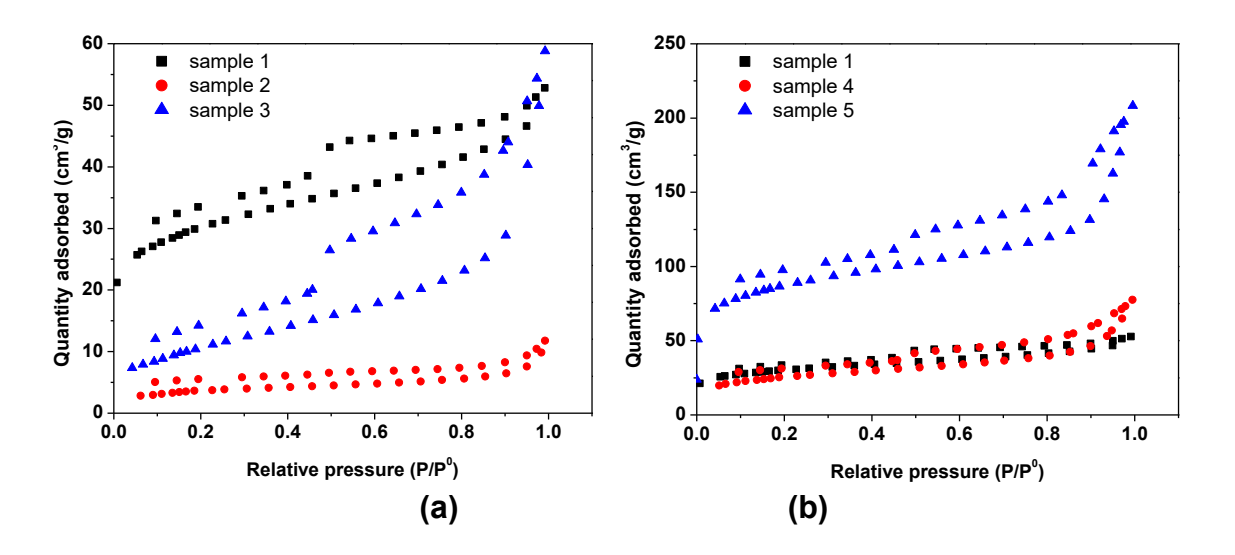
where Q_m (mg/g) is the maximum monolayer adsorption capacity estimated by Langmuir model, K_L (mL/mg) is the Langmuir constant related to the affinity of binding. K_F ((mg/g)(mL/mg)^{1/n}) and 1/n are the Freundlich constants relating adsorption capacity and intensity, respectively.

Pseudo first-order equation:
$$Q_t = q_e(1 - e^{-k_l t})$$
 (S3)

Pseudo second-order equation:
$$Q_t = \frac{tk_2q_e^2}{tk_2q_e + 1}$$
 (S4)

Intraparticle diffusion equation:
$$Q_t = k_i t^{1/2} + C$$
 (S5)

where q_e (mg/g) is the calculated adsorption amount at equilibrium, k_1 (1/min) and k_2 (g/(mg·min)) are the rate constants from the pseudo first-order and pseudo second-order models, respectively, initial adsorption rate is defined as $v_0 = k_2 q_e^2$, k_i (mg/(g.min^{1/2})) is the apparent diffusion rate constant, and C is a constant.



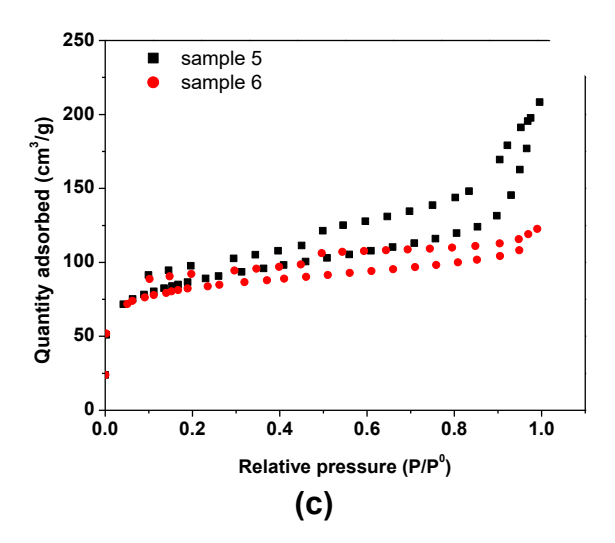


Fig. S1. N_2 adsorption/desorption isotherms of the mesoporous bamboo biochars: (a) samples 1 through 3; (b) samples 1, 4, and 5; (c) samples 5 and 6

Table S1. Model Fitting Parameters of Adsorption Isotherm Data for 2-naphthol at 298 K

		Langmuir Fitting		Freundlich Fitting			
Sample	Q _m (mg/g)	<i>K</i> ∟ (mL/mg)	R ²	<i>K</i> _F (mg/g)(mL/mg) ^{1/n}	1/n	R ²	
1	118.8	0.8835	0.995	63.98	0.796	0.995	
2	-	-	-	122.0	1.18	0.981	
3	-	-	-	126.8	1.25	0.941	
4	5581	0.04412	0.988	235.9	0.974	0.989	
5	168.4	12.09	0.927	198.8	0.348	0.961	
6	125.7	4.322	0.934	127.0	0.502	0.962	

Table S2. Model Fitting Parameters of Adsorption Isotherm Data for BH at 298 K

		Langmuir Fitting		Freundlich Fitting			
Sample	Q _m (mg/g)	<i>K</i> ∟ (mL/mg)	R ²	<i>K</i> _F (mg/g)(mL/mg) ^{1/n}	1/n	R ²	
1	132.5	3.624	0.945	128.0	0.533	0.961	
2	83.46	10.55	0.979	92.07	0.328	0.990	
3	190.4	3.243	0.951	181.2	0.563	0.970	
4	101.8	17.68	0.996	111.6	0.234	0.986	
5	141.6	14.59	0.979	163.2	0.299	0.990	
6	82.77	16.08	0.981	92.58	0.263	0.995	

Table S3. Model Fitting Parameters of Adsorption Isotherm Data for CR at 298 K

		Langmuir Fitting		Freundlich Fitting			
Sample	Q _m (mg/g)	<i>K</i> ∟ (mL/mg)	R ²	<i>K</i> _F (mg/g)(mL/mg) ^{1/n} 1/n		R ²	
1	78.37	7.028	0.993	83.80	0.400	0.999	
2	107.7	4.245	0.934	108.5	0.508	0.957	
3	78.92	6.252	0.990	82.75	0.417	0.986	
4	104.8	4.943	0.957	108.4	0.477	0.973	
5	110.6	29.61	0.969	125.4	0.197	0.985	
6	105.3	4.318	0.984	105.7	0.500	0.995	

Table S4. Model Fitting Parameters of Adsorption Isotherm Data for 2-naphthol, BH, and CR at 298, 308, and 318 K on Sample 5

		Lang	gmuir Fittin	ıg	Freundlich Fitting			
Adsorbate	Temperature (K)	Q _m (mg/g)	<i>K</i> _L (mL/mg)	R ²	K _F (mg/g)(mL/mg) ^{1/n}	1/n	R ²	
	298	168.4	12.09	0.927	198.8	0.348	0.961	
2-naphthol	308	250.2	0.7548	0.985	120.1	0.801	0.989	
	318	3.583 × 10 ⁶	0.00005	0.958	177.6	1.08	0.960	
	298	141.6	14.59	0.979	163.2	0.299	0.990	
BH	308	220.0	1.546	0.952	160.6	0.708	0.960	
	318	1350	0.1569	0.945	172.8	0.859	0.951	
	298	110.6	29.61	0.969	125.4	0.197	0.985	
CR	308	2.742 × 10 ⁷	8.551 × 10 ⁻⁶	0.995	236.3	1.01	0.995	
	318	202.5	1.514	0.983	144.5	0.701	0.988	

_bioresources.cnr.ncsu.edu

Table S5. Model Fitting Parameters of Adsorption Kinetic Data of 2-naphthol, BH, and CR on Sample 5 at 298 K

A 1	Pseudo-first-order Model			Ps	Pseudo-second-order Model			Intraparticle D	iffusion Mo	del
Adsorbate	q _e (mg/g)	k ₁ (1/min)	R ²	q _e (mg/g)	k 2	v₀ (mg/(g.min))	R ²	k _i (mg/(g.min ^{1/2}))	C (mg/g)	R ²
2-naphthol	139.7	0.2849	0.983	143.0	0.00628	128.4	0.988	6.195	79.17	0.439
BH	159.7	0.1637	0.993	167.9	0.00223	-62.85	0.996	12.45	62.11	0.611
CR	122.6	0.06501	0.949	133.8	0.00079	14.15	0.981	6.920	47.48	0.690